Beyond Thermal Management: Incorporating p-Diamond Back-Barriers and Cap Layers Into AlGaN/GaN HEMTs

Yuhao Zhang, *Student Member, IEEE*, Koon Hoo Teo, *Member, IEEE*, and Tomás Palacios, *Senior Member, IEEE*

***Abstract*— This work explores the use of p-diamond back-barriers (BBs) and cap layers to enhance the performance of GaN-based high electron mobility transistors (HEMTs). Diamond can offer a heavily doped p-type layer, which is complementary to GaN electronics. Self-consistent electrothermal simulations reveal that the use of p-diamond BBs and cap layers can increase the breakdown voltage of GaN-based HEMTs by fourfold, at the same time that they enhance the 2-D-electron-gas confinement and reduce short channel effects. These results highlight that p-diamond layers can improve the performance of GaN HEMTs for high-power and high-frequency applications beyond the thermal improvements pursued until now.**

***Index Terms*— GaN high electron mobility transistors (HEMTs), p-diamond back-barrier (BB), p-diamond cap layer, power electronics.**

I. Introduction

GaN-BASED transistors and diodes are excellent candidates for high-voltage and high-frequency electronics. In particular, GaN high electron mobility transistors (HEMTs), which utilize a 2-D-electron-gas (2-DEG) channel, have demonstrated excellent power and frequency performances [1]. High cutoff frequency over 400 GHz [2] and RF output power over 800 W at 2.9 GHz have been demonstrated in GaN HEMTs [3]. However, applications such as radars for air traffic controllers, satellites for broadcasting, and high-power motors require an even higher power (∼kW) at high frequency (e.g., K-band), which are still challenging for GaN HEMTs.

A promising method to further improve the performance of GaN-based HEMTs is to incorporate diamond into the HEMT structure. As shown in Table I, diamond has ∼three times higher critical breakdown field (E_c) and ∼ten times higher thermal conductivity than GaN, and has the highest Baliga's figure of merit (FOM), a key FOM for high-frequency power device performance [4], among all the potential materials listed [5]. In addition, p-type doping is well established in diamond but still challenging in GaN. Boron doping (p-doping) in single-crystal, polycrystalline, and nanocrystalline diamond (NCD) can reach a concentration as high as 10^{18}–10^{21} cm^{-3} [6]–[8] with free hole concentration over 10^{20} cm^{-3} [8], [9]. A hole mobility of 300–600 cm^2/Vs has been demonstrated in p-diamond thanks to hopping transport mechanism [6], [10]. In contrast, the p-doping in GaN has a maximum hole concentration of 10^{17}–10^{18} cm^{-3} and maximum hole mobility still below 30 cm^2/Vs [11], [12].

TABLE I
MATERIAL PROPERTIES OF MAJOR SEMICONDUCTORS CONSIDERED FOR POWER AND MICROWAVE APPLICATIONS

	Si	GaAs	SiC	GaN	Diamond
E_g (eV)	1.1	1.4	3.3	3.4	5.5
μ_e (cm^2/Vs)	1400	8000	1000	2000	2000-4500
μ_h (cm^2/Vs)	600	400	100	850	3000-4000
E_c (MV/cm)	0.3	0.4	2.5	3.3	10
k_T (W/cmK)	1.3	0.46	4.2	1.3-2	10-20
ε	11.8	12.9	9.7	9	5.5
Baliga's FOM $\varepsilon\mu E_c^2$	1	15	340	1450	24664

E_g: bandgap; μ_e, μ_h: electron and hole mobility; E_c: critical electric field; k_T: thermal conductivity; ε: dielectric constant. μ_e of 2DEG is used for GaN.

Recent progress in GaN and diamond growth have made the integration of diamond and GaN devices possible. GaN layers can be epitaxially grown on [13] or wafer-transferred [14], [15] to single-crystal [13] or polycrystalline [14], [15] diamond substrates grown by chemical vapor deposition (CVD). Deposition of NCD coating has also been enabled to passivate GaN devices [16]. However, almost all current diamond and GaN integration merely focus on thermal management, which cannot take full advantage of the complementary properties of GaN and diamond.

In this paper, we propose to incorporate diamond, as an electronic material, into GaN-based power and microwave devices for the first time. p-diamond is proposed to serve as multifunctional back-barriers (BBs) or cap layers for GaN HEMTs. Electrothermal simulation has demonstrated p-diamond capa-

Manuscript received October 9, 2015; accepted April 8, 2016. Date of publication April 22, 2016; date of current version May 19, 2016. Y. Zhang conducted this work while he was working at MERL as an intern. Prof. T. Palacios collaborated with MERL for this research with his related work supported by the ONR PECASE program, monitored by Dr. Paul Maki, and the ARPA-E SWITCHES program, monitored by Dr. Timothy Heidel. The review of this paper was arranged by Editor G. Ghione.

Y. Zhang was with Mitsubishi Electric Research Laboratories, Cambridge, MA 02139 USA. He is now with Microsystems Technology Laboratories, Department of Electrical Engineering and Computer Science, Massachusetts Institute of Technology, Cambridge, MA 02139 USA (e-mail: yhzhang@mit.edu).

K. H. Teo is with Mitsubishi Electric Research Laboratories, Cambridge, MA 02139 USA (e-mail: teo@merl.com).

T. Palacios is with Microsystems Technology Laboratories, Department of Electrical Engineering and Computer Science, Massachusetts Institute of Technology, Cambridge, MA 02139 USA (e-mail: tpalacios@mit.edu).

Color versions of one or more of the figures in this paper are available online at http://ieeexplore.ieee.org.

Digital Object Identifier 10.1109/TED.2016.2553136

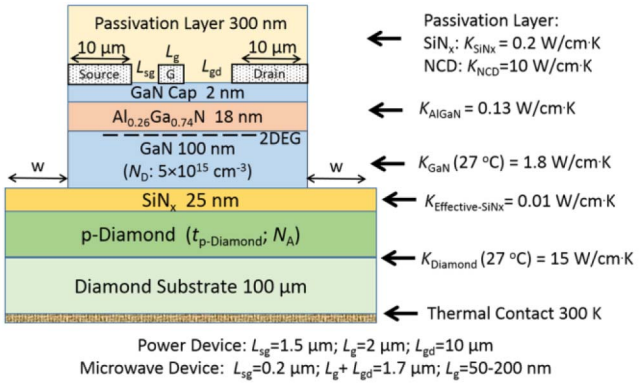

Fig. 1. Schematic of GaN-on-diamond HEMTs with a p-diamond BB. Thermal conductivity of different layers and thermal contact settings are also listed. Two sets of source-to-gate distance (L_{sg}), gate length (L_g), and gate-to-drain distance (L_{gd}) are selected to simulate power and microwave devices.

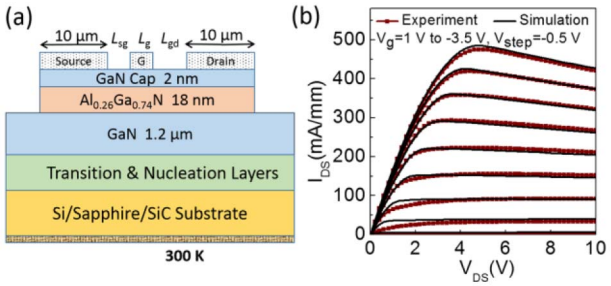

Fig. 2. (a) Schematic of the fabricated AlGaN/GaN HEMT structures on Si/Sapphire/SiC substrates that were used for simulation model calibration. (b) Comparison between simulation and experimental dc output characteristics for a single-finger GaN-on-Si HEMT.

bility in enhancing breakdown voltage (BV), thermal performance, and 2-DEG confinement for GaN HEMTs.

II. p-DIAMOND AS A MULTIFUNCTIONAL BACK-BARRIER

The schematic of the GaN-on-diamond HEMT with a p-diamond BB is shown in Fig. 1. The AlGaN/GaN HEMT layers are based on the GaN-on-Si HEMTs fabricated at MIT [17], [18], consisting of 2-nm GaN cap, 18-nm $Al_{0.26}Ga_{0.74}N$, and 100-nm unintentionally doped GaN (background doping $N_D \sim 5 \times 10^{15}$ cm^{-3}). The 2-DEG density was revealed by Hall measurement as 1.25×10^{13} cm^{-2}. The GaN-on-diamond wafer structure is based on the experimental demonstration reported in [14] and [15], where the GaN layers were extracted from epitaxial GaN-on-Si wafers, followed by the CVD growth of p-diamond BB and 100-μm diamond substrate on top of a ~25-nm intermediate SiN_x dielectric layer. The p-diamond BB thickness and doping concentration are denoted by $t_{\mathrm{p-Diamond}}$ and N_A, respectively. Two sets of source-to-gate distance (L_{sg}), gate length (L_g), and gate-to-drain distance (L_{gd}) are selected to simulate power (Part II B and II C) and microwave devices (Part II D), as shown in Fig. 1.

A. Simulation Model and Calibration

The self-consistent electrothermal simulations were performed using the Silvaco ATLAS simulator [19], based on the simulation models previously developed for GaN lateral and vertical power devices at MIT [17]. A thermal diffusion region (width $w = 500$ μm) was added for single-finger device simulation and an adiabatic thermal boundary condition was added at the unit-cell sidewall to enable the multifinger device simulation [17]. The thermal conductivity of different materials in device is listed in Fig. 1. Both NCD (10 W/cm · K [20]) and SiN_x (0.2 W/cm · K) are considered for device passivation. The thermal conductivity of GaN and CVD-grown polycrystalline diamond was set as 1.8 and 15 W/cm · K [14], with a temperature dependence model described in [17]. An effective thermal conductivity of 0.01 W/cm · K for SiN_x transitional dielectrics was calculated from the reported thermal boundary resistance in GaN-on-diamond structures [14]. The diamond bandgap and relative permittivity was set as 5.5 eV and 5.5, respectively; the electron affinity was set as 0.35 eV for a clean reconstructed diamond surface after releasing hydrogen-termination [21] and SiN_x passivation. p-diamond carrier concentration and mobility are based on experimental reports in [8].

The electrothermal models were calibrated and verified by utilizing the HEMT structure on Si/sapphire/SiC substrates fabricated at MIT, as shown in Fig. 2(a). Excellent agreement between experiment and simulation was observed for all devices. A typical comparison between simulation and experimental dc I–V characteristics is shown in Fig. 2(b).

B. Breakdown Voltage Enhancement

The insertion of p-diamond BB can enhance device BV by forming a reduced surface field (RESURF) structure. The p-diamond/n-GaN junction below the 2-DEG channel can deplete the channel by a vertical electric field (E-field) at OFF-state and thus spread the horizontal E-field. As shown in the simulated E-field distribution of GaN HEMTs without and with a p-GaN BB [Fig. 3(a) and (b)], the p-diamond/n-GaN junction greatly reduces the E-field peak at the gate edge and enables an almost uniform E-field distribution in GaN and diamond between gate and drain. The peak E-field in $Al_{0.26}Ga_{0.74}N$ and GaN was reduced from 15 and 8 MV/cm, much higher than the E_c of GaN (3.4 MV/cm) and $Al_{0.26}Ga_{0.74}N$ (5.5 MV/cm for a bandgap of 3.96 eV [22]), to 4.8 and 2.8 MV/cm, at a reverse bias of $V_{GS} = -5$ V and $V_{DS} = 1250$ V.

The RESURF design principle for HEMTs is to completely deplete the 2-DEG charge by the p-n junction at breakdown [23]. In the optimized design, two equal E-field peaks would appear at the gate and drain edges [24], as shown in Fig. 3(b). In the case of charge unbalance, if p-diamond charges are not enough to deplete 2-DEG, then a higher E-field peak would appear at the gate edge [Fig. 3(c)]; if p-diamond charges are more than 2-DEG, then the p-n junction would induce a higher E-field peak at the drain edge [Fig. 3(d)].

In simulation, device BV was extracted when the peak E-field in any region reaches the E_c of corresponding material [17]. The E_c of GaN, $Al_{0.26}Ga_{0.74}N$, diamond, and

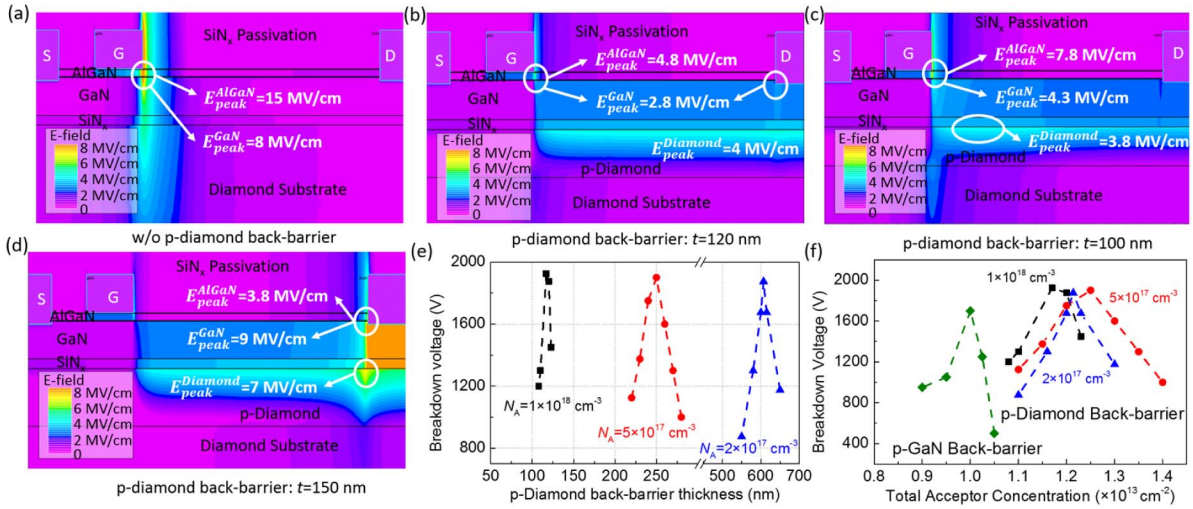

Fig. 3. Simulated electric field distribution in GaN-on-diamond HEMTs (a) without a p-diamond BB and with (b) 120-nm-, (c) 100-nm-, and (d) 150-nm-thick p-diamond BB, all at an OFF-state bias of $V_{GS} = -5$ V and $V_{DS} = 1250$ V. The locations of peak E-field in main regions are denoted. (e) BV dependence on p-diamond BB thickness at three different p-diamond doping levels. (f) BV dependence on total acceptor concentration for p-GaN and p-diamond BB.

SiN_x were set as 3.4, 5.5, 7 (reported for CVD polycrystalline diamond [25]), and 10 MV/cm, respectively. As shown in Fig. 3(e), a maximum BV of ~1.9 kV can be achieved by different p-diamond doping concentrations N_A, with different optimized p-diamond BB thicknesses t correspondingly. As shown in Fig. 3(f), all these optimized N_A and t correspond to the similar total charge density ($N_A \cdot t$) equivalent to the 2-DEG density, showing the strong charge balance effect aforementioned. The maximum ~1.9 kV BV is larger than the ~500 V and ~1.65 kV BV of GaN HEMTs without BB and with a p-GaN BB (all with $L_{gd} = 10$ μm), demonstrating the effectiveness of p-diamond BB in BV enhancement.

Under perfect charge balance, a patterned p-diamond BB can further reduce the peak E-field at the drain edge, with the BB edge sitting between gate and drain. Fig. 4(a) shows the E-field distribution in an HEMT with a patterned p-diamond BB, where the edge of BB is 1.5 μm away from the drain edge horizontally. From the comparison of Figs. 3(b) and 4(a), it can be seen that the patterned p-diamond BB moves the peak E-field location in GaN from the drain edge to the p-diamond/n-GaN junction, creating a more spread E-field distribution in GaN and therefore enabling a higher BV of over 2500 V for $L_{gd} = 10$ μm. The dependence of BV on the patterned p-diamond BB length is shown in Fig. 4(b), revealing an optimized length L_{BB}^{opt} for maximum BV. The breakdown will occur at the gate edge when the BB length $L_{BB} < L_{BB}^{opt}$, and at drain edge if $L_{BB} > L_{BB}^{opt}$. This E-field modulation effect was not observed for p-GaN BB, where the peak E-field in GaN always stays near the 2-DEG channel rather than moves toward p-n junction and the BV reaches maximum when BB extends to the drain side [Fig. 4(b)]. This is probably due to the relatively small vertical E-field in GaN p-n junctions compared to that in the p-diamond/n-GaN junction.

It should also be noted that the introduction of p-diamond BB does not deteriorate the device forward characteristics. Simulations have revealed only a ~5% ON-resistance increase

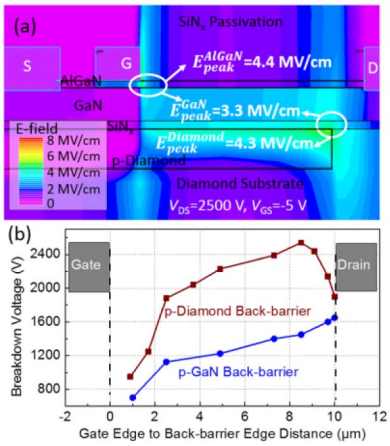

Fig. 4. (a) Simulated electric field distribution in GaN-on-diamond HEMTs with a patterned p-diamond BB, at the bias of $V_{GS} = -5$ V and $V_{DS} = 2500$ V. The gate edge to BB edge distance is 8.5 μm. (b) Dependence of device BV on the gate edge to BB edge distance for GaN HEMTs with p-diamond and p-GaN BBs. The geometry and doping of p-GaN and p-diamond BB are extracted from Fig. 3(f) for a charge balance condition with 2-DEG.

due to the partial depletion of 2-DEG by p-diamond BB at ON-state. For patterned p-diamond BBs with different lengths (Fig. 4), the ON-resistance difference is within ~3% from the simulation.

C. Thermal Performance Enhancement

In practical applications, the device peak temperature T_{peak} is limited to, for example, 150 °C or 200 °C, ensure long-term reliable operation. This peak temperature limit determines the device maximum allowable power dissipation [17]. Thus, power ~T_{peak} dependence was simulated to present and compare device thermal performance.

From the simulated lattice temperature distribution shown in Fig. 5, it can be seen that the T_{peak} locates at the gate edge

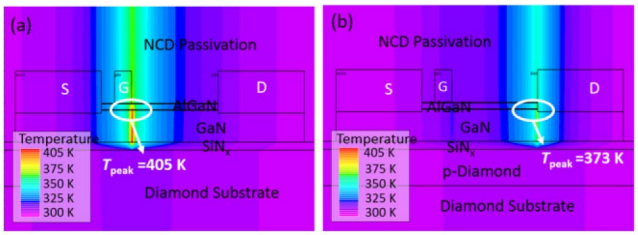

Fig. 5. Simulated lattice temperature distribution in GaN-on-diamond HEMTs (a) without and (b) with a p-diamond BB, at an ON-state bias of $V_{GS} = 0$ V and $V_{DS} = 30$ V. The peak temperature and its location are denoted.

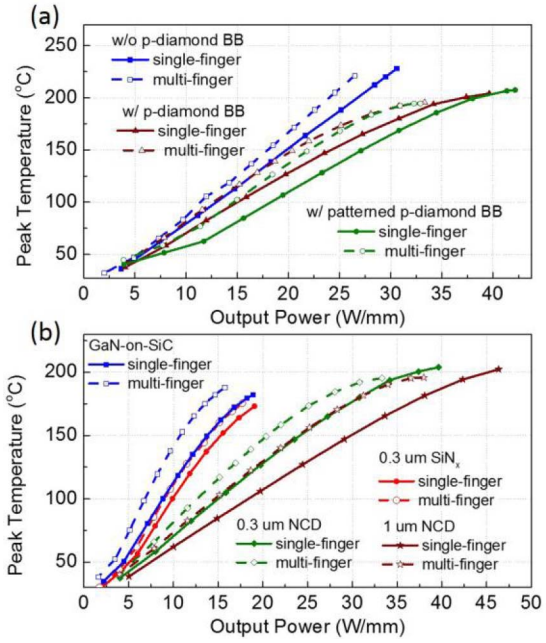

Fig. 6. Simulated peak temperature dependence on output power density for (a) GaN-on-diamond HEMTs with and without a p-diamond BB and with an optimized patterned p-diamond BB and (b) GaN-on-SiC HEMTs with 0.3-μm SiN_x passivation and GaN-on-diamond HEMTs with 0.3-μm SiN_x, 0.3-μm NCD, and 1-μm NCD passivation. Single-finger and multifinger simulations for all devices are conducted.

in GaN HEMTs without a p-diamond BB and at the drain edge in GaN HEMTs with a p-diamond BB, as a result of the combination of high E-field and high current density [17] at each location. In addition, a lower T_{peak} is observed in GaN HEMTs with a p-diamond BB at the same bias, due to the E-field relaxation by p-diamond BB discussed in the last section. An even lower T_{peak} is observed in GaN HEMTs with an optimized patterned p-diamond BB. Fig. 6(a) shows the power $\sim T_{peak}$ dependence for these three devices with the same material structure but different E-field distributions. For $T_{peak} = 150$ °C, ~23% higher power density can be achieved by the introduction of p-diamond BB and ~35% higher power by the optimized patterned p-diamond BB.

The influence of the layer structure on the thermal performance was also studied. As shown in Fig. 6(b), the power $\sim T_{peak}$ performance of the GaN-on-diamond HEMTs with the same p-diamond BB but different passivation layers was simulated and benchmarked with respect to a GaN-on-SiC device [structure shown in Fig. 2(a)]. As shown for $T_{peak} = 150$ °C, although the thermal conductivity of polycrystalline diamond is almost four times the one of SiC, only ~15% higher power density was achieved in GaN-on-diamond than GaN-on-SiC. The relative small thermal improvement is due to the large thermal boundary resistance of the intermediate dielectric layer used between diamond and GaN [14]. This difference could be even smaller if the thermal conductivity of thin p-diamond layers is lower than the one used in the simulations, taken from thick diamond substrates. However, if the surface passivation material changes from 0.3-μm SiN_x to 0.3-μm NCD, a ~50% power density increase can be achieved. If the thickness of NCD passivation increases from 0.3 to 1 μm, a power density over 30 W/mm, more than two times that of GaN-on-SiC, can be achieved for $T_{peak} = 150$ °C. These results illustrate the great potential of NCD passivation in the thermal management of GaN power devices.

D. High-Frequency Performance Enhancement

In GaN-based microwave devices, the gate length is typically scaled down below 200 nm. The short gate length causes short-channel effects such as threshold-voltage (V_{th}) shift, soft pinchoff, and high subthreshold current [26]. A BB structure with high bandgap (e.g., AlGaN [27]) or large polarization charges (e.g., InGaN [26]) has been proved as an effective solution for reducing short-channel effects and enhancing 2-DEG confinement.

With a larger bandgap than GaN and p-type doping, p-diamond BB can form a large potential barrier that opposes the movement of electrons from 2-DEG toward buffer layers, as shown in the simulated band diagram [Fig. 7(a)]. Thanks to the larger energy barrier formed by p-diamond compared with conventional AlGaN BB, short-gate GaN HEMTs with p-diamond BB show not only a much smaller V_{th} shift but also a significant improvement in the subthreshold slope, as shown in Fig. 7(b). The enhanced suppression of V_{th} shift by p-diamond BB is more remarkable for shorter gate and higher frequency devices, as shown in the simulated DIBL (defined as $\Delta V_{th}/\Delta V_{DS}$ and V_{DS} of 1 and 10 V used in our simulation) as a function of gate length for GaN HEMTs with different BBs [Fig. 7(c)].

Device transfer characteristics were then simulated in ac mode and transconductance g_m and gate capacitances C_{gd} and C_{gs} were extracted as a function of V_{GS}. The intrinsic cutoff frequency f_T was calculated by $f_T = (g_m/2\pi(C_{gs} + C_{gd}))$ for each V_{GS} and the peak f_T was extracted [28]. As shown in Fig. 7(d), a slightly higher f_T is observed in GaN HEMTs with p-diamond BBs, indicating that the incorporation of p-diamond BBs does not diminish device frequency performances. To further compare the BV $\sim$ f_T tradeoff for microwave devices, HEMTs with a gate field plate (FP) are also simulated, as FP is a widely used method to increase BV. The FP geometry was optimized according to [29]. The FP increases the BV from ~100 to ~250 V (L_{sg}, L_g, and L_{gd} shown in Fig. 1 for microwave device), but introduces additional gate capacitance [29] and greatly

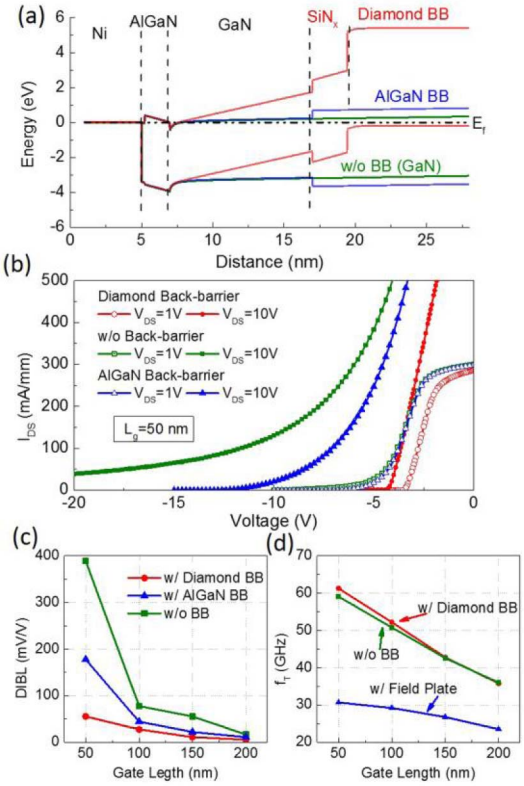

Fig. 7. Simulated (a) band-diagram and (b) transfer characteristics of GaN HEMTs without BB, with a p-diamond BB, and with an AlGaN BB. (c) Calculated DIBL of the three devices for gate lengths of 50, 100, 150, and 200 nm. (d) Simulated peak f_T of GaN-on-diamond HEMTs with and without p-diamond BB and with an optimized FP structure. The ac simulation was conducted at $f = 1$ MHz. All the device simulated in this section utilized L_{sg}, L_g, and L_{gd} of the microwave device illustrated in Fig. 1.

reduces the device f_T [Fig. 7(d)]. In contrast, GaN HEMTs with a p-diamond BB, with a ~400 V BV and >60-GHz f_T, outperform the HEMTs with and without an FP in both BV and f_T.

It should be noted that trapping effects have not been considered in our ac simulation, as negligible current collapse has been reported in GaN HEMTs with either diamond substrates [12] or NCD passivation [13]. In addition, the large potential barrier formed by p-diamond BBs would also reduce the possible electron trapping at GaN/SiN_x/diamond interfaces. Thus, we do not expect the trapping effects to significantly diminish the greatly enhanced BV ~ f_T tradeoff in GaN HEMTs with a p-diamond BB. Also, parasitic access resistance and capacitances have not been considered in our simulation. For sub-50-nm gate devices, they need to be considered for accurate device cutoff frequency calculation.

III. p-Diamond as a Multifunctional Cap Layer

Besides a BB, p-diamond can serve as a multifunctional cap layer in GaN HEMTs, to enhance BV ~ R_{ON} tradeoff and thermal performance [Fig. 8(a)]. p-diamond cap layer can be grown by CVD on the top of dielectric-coated AlGaN/GaN epilayers [14], [15], or possibly deposited by NCD coating [16] following with a p-type doping in NCD [8]. Then the p-diamond can be partially patterned. Gate electrodes

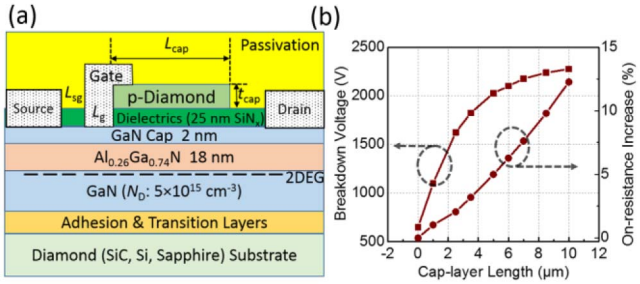

Fig. 8. (a) Schematic of the GaN HEMTs with a p-diamond cap layer. The L_{sg}, L_g, and L_{gd} are set as 1.5, 2, and 10 μm. (b) Dependence of BV and ΔR_{ON} as a function of cap-layer length L_{cap}. The cap-layer thickness t_{cap} and doping level are 60 nm and 1×10^{18} cm^{-3}.

form a Schottky contact to the GaN cap layer and can form either a Schottky or an Ohmic contact (similar to the device in [30] for the Ohmic contact) on the p-diamond cap layer.

Similar to p-diamond BB, p-diamond cap layer can also compensate 2-DEG at OFF-state to enable a more uniform E-field distribution and a higher BV. Besides total charge amount, a large modulation effect by cap-layer length was also observed for device BV and R_{ON}. As shown in Fig. 8(b), with the p-diamond length extending from gate to drain, a ~3.5 times higher BV can be achieved at the cost of a ~12% higher R_{ON}. A great improvement in thermal performance is also seen in GaN HEMTs with p-diamond cap layers, due to relaxed E-field distribution and diamond surface heat spreaders. Similar to the results shown in Fig. 6(b), an additional NCD passivation layer would give the best thermal performance. In addition, the p-diamond cap layer, though may not be so effective in enhancing 2-DEG confinement as p-diamond BBs, is expected to reduce the electron trapping in AlGaN layer and GaN surface by vertical E-field. This is especially beneficial to GaN high-voltage power devices, as the surface and AlGaN trapping is a critical issue in these devices.

IV. Conclusion

In this paper, we propose new concepts for the integration of p-diamond BBs and cap layers into AlGaN/GaN HEMTs. These new devices take advantage of the complementary electrical properties of diamond and GaN. Electrothermal simulations have demonstrated a large enhancement in the BV, thermal performance, 2-DEG confinement, and a reduction of short-channel effects by p-diamond BBs or cap layers. These results show great potential of incorporating p-diamond layers into GaN HEMTs for high-power and high-frequency applications.

References

[1] R. S. Pengelly, S. M. Wood, J. W. Milligan, S. T. Sheppard, and W. L. Pribble, "A review of GaN on SiC high electron-mobility power transistors and MMICs," *IEEE Trans. Microw. Theory Techn.*, vol. 60, no. 6, pp. 1764–1783, Jun. 2012.

[2] K. Shinohara *et al.*, "Self-aligned-gate GaN-HEMTs with heavily-doped n^+-GaN ohmic contacts to 2DEG," in *Proc. IEEE Int. Electron Devices Meeting (IEDM)*, Dec. 2012, pp. 27.2.1–27.2.4.

[3] E. Mitani, M. Aojima, A. Maekawa, and S. Sano, "An 800-W AlGaN/GaN HEMT for S-band high-power application," in *CSMantech On-Line Dig.*, 2007, pp. 213–216.
[4] B. J. Baliga, "Power semiconductor device figure of merit for high-frequency applications," *IEEE Electron Device Lett.*, vol. 10, no. 10, pp. 455–457, Oct. 1989.
[5] C. J. H. Wort and R. S. Balmer, "Diamond as an electronic material," *Mater. Today*, vol. 11, nos. 1–2, pp. 22–28, Jan./Feb. 2008.
[6] R. Kalish, "Doping of diamond," *Carbon*, vol. 37, no. 5, pp. 781–785, 1999.
[7] S. Yamasaki *et al.*, "Potential of diamond power devices," in *Proc. 25th Int. Symp. Power Semiconductor Devices ICs (ISPSD)*, May 2013, pp. 307–310.
[8] W. Gajewski *et al.*, "Electronic and optical properties of boron-doped nanocrystalline diamond films," *Phys. Rev. B*, vol. 79, no. 4, p. 045206, Jan. 2009.
[9] M. Werner *et al.*, "The relationship between resistivity and boron doping concentration of single and polycrystalline diamond," *Phys. Status Solidi A*, vol. 154, no. 1, pp. 385–393, Mar. 1996.
[10] S. Koizumi, K. Watanabe, M. Hasegawa, and H. Kanda, "Ultraviolet emission from a diamond pn junction," *Science*, vol. 292, no. 5523, pp. 1899–1901, Jun. 2001.
[11] U. Kaufmann, P. Schlotter, H. Obloh, K. Köhler, and M. Maier, "Hole conductivity and compensation in epitaxial GaN:Mg layers," *Phys. Rev. B*, vol. 62, no. 16, p. 10867, 2000.
[12] I. P. Smorchkova *et al.*, "Mg doping of GaN layers grown by plasma-assisted molecular-beam epitaxy," *Appl. Phys. Lett.*, vol. 76, no. 6, pp. 718–720, Feb. 2000.
[13] K. Hirama, M. Kasu, and Y. Taniyasu, "RF high-power operation of AlGaN/GaN HEMTs epitaxially grown on diamond," *IEEE Electron Device Lett.*, vol. 33, no. 4, pp. 513–515, Apr. 2012.
[14] J. Pomeroy *et al.*, "Achieving the best thermal performance for GaN-on-diamond," in *Proc. IEEE Compound Semiconductor Integr. Circuit Symp. (CSICS)*, Oct. 2013, pp. 1–4.
[15] D. C. Dumka *et al.*, "Electrical and thermal performance of AlGaN/GaN HEMTs on diamond substrate for RF applications," in *Proc. IEEE Compound Semiconductor Integr. Circuit Symp. (CSICS)*, Oct. 2013, pp. 1–4.
[16] D. J. Meyer *et al.*, "Large-signal RF performance of nanocrystalline diamond coated AlGaN/GaN high electron mobility transistors," *IEEE Electron Device Lett.*, vol. 35, no. 10, pp. 1013–1015, Oct. 2014.
[17] Y. Zhang *et al.*, "Electrothermal simulation and thermal performance study of GaN vertical and lateral power transistors," *IEEE Trans. Electron Devices*, vol. 60, no. 7, pp. 2224–2230, Jul. 2013.
[18] Y. Zhang, M. Sun, S. J. Joglekar, T. Fujishima, and T. Palacios, "Threshold voltage control by gate oxide thickness in fluorinated GaN metal-oxide-semiconductor high-electron-mobility transistors," *Appl. Phys. Lett.*, vol. 103, no. 3, p. 033524, Jul. 2013.
[19] *ATLAS User's Manual*, Silvaco Int., Santa Clara, CA, USA, 2008.
[20] A. Wang, M. J. Tadjer, and F. Calle, "Simulation of thermal management in AlGaN/GaN HEMTs with integrated diamond heat spreaders," *Semicond. Sci. Technol.*, vol. 28, no. 5, p. 055010, May 2013.
[21] J. Robertson and M. J. Rutter, "Band diagram of diamond and diamond-like carbon surfaces," *Diamond Rel. Mater.*, vol. 7, nos. 2–5, pp. 620–625, Feb. 1998.
[22] A. Nishikawa, K. Kumakura, and T. Makimoto, "High critical electric field exceeding 8 MV/cm measured using an AlGaN p-i-n vertical conducting diode on n-SiC substrate," *Jpn. J. Appl. Phys.*, vol. 46, no. 4B, p. 2316, Apr. 2007.
[23] S. Karmalkar, J. Deng, M. S. Shur, and R. Gaska, "RESURF AlGaN/GaN HEMT for high voltage power switching," *IEEE Electron Device Lett.*, vol. 22, no. 8, pp. 373–375, Aug. 2001.
[24] J. A. Appels and H. M. J. Vaes, "High voltage thin layer devices (RESURF devices)," in *Proc. Int. Electron Devices Meeting*, vol. 25. 1979, pp. 238–241.
[25] C. A. Klein and R. DeSalvo, "Thresholds for dielectric breakdown in laser-irradiated diamond," *Appl. Phys. Lett.*, vol. 63, no. 14, pp. 1895–1897, Oct. 1993.
[26] T. Palacios, A. Chakraborty, S. Heikman, S. Keller, S. P. DenBaars, and U. K. Mishra, "AlGaN/GaN high electron mobility transistors with InGaN back-barriers," *IEEE Electron Device Lett.*, vol. 27, no. 1, pp. 13–15, Jan. 2006.
[27] D. S. Lee, X. Gao, S. Guo, and T. Palacios, "InAlN/GaN HEMTs with AlGaN back barriers," *IEEE Electron Device Lett.*, vol. 32, no. 5, pp. 617–619, May 2011.
[28] S. Adak, A. Sarkar, S. Swain, H. Pardeshi, S. K. Pati, and C. K. Sarkar, "High performance AlInN/AlN/GaN p-GaN back barrier gate-recessed enhancement-mode HEMT," *Superlattices Microstruct.*, vol. 75, pp. 347–357, Nov. 2014.
[29] S. Karmalkar and U. K. Mishra, "Enhancement of breakdown voltage in AlGaN/GaN high electron mobility transistors using a field plate," *IEEE Trans. Electron Devices*, vol. 48, no. 8, pp. 1515–1521, Aug. 2001.
[30] A. Nakajima, Y. Sumida, M. H. Dhyani, H. Kawai, and E. M. S. Narayanan, "GaN-based super heterojunction field effect transistors using the polarization junction concept," *IEEE Electron Device Lett.*, vol. 32, no. 4, pp. 542–544, Apr. 2011.

Yuhao Zhang (S'13) received the B.S. degree in physics from Peking University, Beijing, China, in 2011, and the M.S. degree in electrical engineering from the Massachusetts Institute of Technology, Cambridge, MA, USA, in 2013, where he is currently pursuing the Ph.D. degree in electrical engineering.

His current research interest includes simulation, modeling, fabrication, and characterization of III–V power electronics.

Koon Hoo Teo (M'06) received the M.S. and Ph.D. degrees in electrical engineering from the University of Alberta, Edmonton, AB, Canada, in 1985 and 1990, respectively.

He is currently with Mitsubishi Electric Research Laboratories, Cambridge, MA, USA. He has authored or co-authored over 80 reviewed papers and 145 granted patents and patent applications.

Tomás Palacios (S'98–M'06–SM'12) is currently an Associate Professor with the Department of Electrical Engineering and Computer Science, Massachusetts Institute of Technology, Cambridge, MA, USA.

His current research include novel devices for information technology, biosensors, and energy conversion. He has authored over 200 papers, three book chapters and eight patents.